Integrin-targeted imaging and therapy with RGD4C-TNF fusion protein

Hui Wang, Kai Chen, Weibo Cai, Zibo Li, Lina He, Amir Kashefi, and Xiaoyuan Chen

Molecular Imaging Program at Stanford, Department of Radiology and Bio-X Program, Stanford University School of Medicine, Stanford, California

Abstract

This study used integrin $\alpha_v\beta_3$ as a target for tumor-specific delivery of tumor necrosis factor-α (TNF). The fusion protein RGD4C-TNF bound specifically to $\alpha_v\beta_3$ as evidenced by cell receptor binding assay and noninvasive micro-positron emission tomography imaging. ^{64}Cu-DOTA-RGD4C-TNF had significantly higher activity accumulation in integrin-positive tumors (U87MG and MDA-MB-435) but not in integrin-negative tumors (C6) compared with ^{64}Cu-DOTA-TNF. The magnitude of tumor uptake of ^{64}Cu-DOTA-RGD4C-TNF correlated well with the $\alpha_v\beta_3$ level (U87MG > MDA-MB-435 > C6). Tumor accumulation of ^{64}Cu-DOTA-RGD4C-TNF could be effectively blocked by c(RGDyK) peptide in $\alpha_v\beta_3$-positive tumor models, suggesting $\alpha_v\beta_3$ specificity of RGD4C-TNF fusion protein *in vivo*. Furthermore, although the fusion of RGD4C moiety to TNF had little effect on the bioactivity and cytotoxicity of RGD4C-TNF compared with TNF in cell culture, RGD4C-TNF was significantly more potent than TNF in inhibiting orthotopic MDA-MB-435 tumor growth. *Ex vivo* tissue staining confirmed specific cytotoxicity of RGD4C-TNF against integrin-positive tumor cells and tumor vasculature. [Mol Cancer Ther 2008;7(5):1044–53]

Introduction

Tumor necrosis factor-α (TNF) is a pleiotropic cytokine with a wide variety of biological activities and immunomodulatory properties (1). Although systemic administration has been shown to mediate the regression of xenotransplanted tumors (2–4), the clinical use of TNF is hindered by its severe dose-limiting toxicity (5, 6). Among the various approaches that have been pursued to increase the therapeutic index, regional administration of high-dose TNF, in combination with chemotherapeutics, has produced high response rates in patients with melanoma and sarcoma of the extremities (7–9) as well as regression of bulky hepatic cancer confined to liver (10, 11). These results are important because they show that the antitumor effects of TNF can be exploited therapeutically in humans with greater success if sufficient dose can be attained locally, which can shield the organism from the systemic toxic effects of TNF. These results also provide the rationale for targeting tumors with TNF as a strategy for increasing its therapeutic index.

Through molecular engineering, numerous fusion proteins have been designed to combine the specific cell-binding characteristics of antibodies or growth factors with the cytotoxic or growth-modulatory effects of toxins, cytokines, or proapoptotic proteins (12, 13). Among these strategies, antibodies have shown the greatest potential thus far as delivery vehicles for various classes of therapeutic agents, including TNF. However, a major limitation of such antibody-based constructs is their inadequate uptake and poor distribution in tumors due in part to the relatively large molecular mass of antibody molecules. One approach to remedy this is to use considerably smaller, genetically engineered antibody fragments. For example, single-chain Fv fusion constructs can better penetrate tumor tissue and have improved pharmacokinetics and lower immunogenicity than intact murine antibodies (14, 15). To further improve the penetration of targeted molecule, we and others have used small peptides for tumor vasculature-specific delivery to enhance the therapeutic index of TNF (16–20).

The integrin $\alpha_v\beta_3$ is overexpressed on endothelial cells of neovasculature and has been shown to play a key role in tumor angiogenesis and metastasis. Overexpression of integrin $\alpha_v\beta_3$ in tumor cells of various origins (21) can potentiate metastasis by facilitating cancer cell invasion and movement across blood vessels. Several integrin inhibitors are being evaluated in clinical trials for cancer and other angiogenesis-related diseases. Currently, patients with melanoma and glioblastoma multiforme benefit from Vitaxin (MedImmune) or cilengitide treatment, respectively (22). Small interfering RNAs that specifically silence integrin α_v and/or β_3 have been reported to cause tumor shrinkage in preclinical xenograft models (23). Combinations of anti-integrin $\alpha_v\beta_3$ therapy and other therapeutic approaches (such as chemotherapy, radiotherapy, and gene therapy) have also been applied to cancer treatment (24). Despite the broad theoretical effect of such molecules on

Received 9/17/07; revised 1/18/08; accepted 2/4/08.

Grant support: National Cancer Institute grants R21 CA102123, R21 CA121842, P50 CA114747, R24 CA93862, and U54 CA119367 and Department of Defense grants W81XWH-04-1-0697, W81XWH-06-1-0665, W81XWH-06-1-0042, and W81XWH-07-1-0374.

The costs of publication of this article were defrayed in part by the payment of page charges. This article must therefore be hereby marked *advertisement* in accordance with 18 U.S.C. Section 1734 solely to indicate this fact.

Requests for reprints: Xiaoyuan Chen, Molecular Imaging Program at Stanford, Department of Radiology and Bio-X Program, Stanford University School of Medicine, 1201 Welch Road, P095, Stanford, CA 94305-5484. Phone: 650-725-0950; Fax: 650-736-7925. E-mail: shawchen@stanford.edu

doi:10.1158/1535-7163.MCT-07-2084

integrin function and thus on pathology, the clear identification of discrete clinical niches for their use remains to be defined. The ability of noninvasive molecular imaging to visualize and quantify integrin expression *in vivo* may provide a novel way of patient stratification and identify integrin-positive patients who will likely benefit from such targeted therapy.

In this study, we developed a RGD4C-TNF fusion protein for tumor-specific delivery of TNF. To investigate whether RGD4C-TNF protein can specifically bind to $\alpha_v\beta_3$-positive cells and thus increase the local concentration of cytotoxic RGD4C-TNF, RGD4C-TNF was conjugated with macrocyclic chelating agent DOTA and labeled with ^{64}Cu for micro-positron emission tomography (microPET) imaging in tumor models with different $\alpha_v\beta_3$ expression levels. The tumor-inhibitory effects of RGD4C-TNF and TNF were studied using an integrin $\alpha_v\beta_3$-positive MDA-MB-435 human breast cancer model.

Materials and Methods

All commercially available chemical reagents were used without further purification. ^{64}Cu [half-life ($t_{1/2}$) = 12.7 h, β^+ = 655 keV (17.4%), β^- = 573 keV (30%)] was obtained from the University of Wisconsin-Madison. [^{125}I]echistatin, specific activity of 74,000 GBq/mmol, was purchased from GE Healthcare. Female athymic nude mice were supplied from Harlan at age 4 to 6 weeks. The enzymes for DNA cloning were purchased from New England Biolabs. The plasmid pBV220 containing the P_RP_L promoters, two strong transcription terminators, and the hTNF cDNA were constructed in-house. Mouse anti-human TNFR1 and TNFR2 were purchased from R&D Systems. RGD4C peptide (ACDCRGDCFCG) was purchased from AnaSpec.

Cell Culture and Tumor Models

All the cell lines used for *in vitro* and *in vivo* studies were obtained from the American Type Culture Collection. U87MG human glioblastoma cells were cultured in MEM supplemented with 2 mmol/L L-glutamine, 1.5 g/L sodium bicarbonate, 0.1 mmol/L nonessential amino acids, 1.0 mmol/L sodium pyruvate, and 10% fetal bovine serum. MDA-MB-435 human breast cancer cells were cultured in Leibovitz's L-15 medium supplemented with 10% fetal bovine serum. C6 rat glioma cells were cultured in RPMI 1640 supplemented with 10% fetal bovine serum. Mouse fibroblast L929 cells were cultured in DMEM (low glucose) supplemented with 10% fetal bovine serum. All cell lines were cultured at 37°C in a humidified atmosphere with 5% CO_2, except for MDA-MB-435, which was cultured without CO_2.

Animal procedures were done according to a protocol approved by the Stanford University Institutional Animal Care and Use Committee. The U87MG tumor model was generated by s.c. injections of 1×10^7 cells in 100 μL PBS into the left shoulders of the mice. The orthotopic MDA-MB-435 tumor model was established by injections of 5×10^6 cells in 100 μL PBS into the right upper mammary fat pads of the mice. The C6 tumor model was generated by s.c. injections of 5×10^6 cells in 100 μL PBS into the left shoulders of the mice. The mice were subjected to micro-PET imaging studies when the tumor volume was between 200 and 500 mm^3.

Production and Characterization of Human TNF and RGD4C-TNF

Wild-type human TNF (hTNF) and RGD4C-TNF (where RGD4C denotes the sequence of CDCRGDCFC) were prepared by recombinant DNA technology. For amplification by PCR, we used the primer pair 5′-GAATTCATGCG-CAAACGTAAGCCTGTA-3′ and 5′-TCAGAAGGCAAT-GATCCC-3′ for hTNF, with an *Eco*RI recognition site at 5′-terminal. Optimal PCR conditions were 30 cycles of 30 s at 96°C, 30 s at 58°C, and 1 min at 72°C. PCR products were visualized on 2% agarose/Tris-acetate EDTA gels. After being confirmed by DNA sequencing, the gene was cloned into prokaryotic expression vector pBV220 (pBV-TNF). To generate fusion gene encoding RGD4C-TNF, the oligonucleotide encoding RGD4C with a glycine-serine linker interposed between RGD4C and TNF as a spacer was synthesized. Both TNF and RGD4C-TNF proteins were expressed and purified using our previously reported method (20).

In vitro Cytolytic Assay of TNF and RGD4C-TNF

The cytolytic activity of TNF and RGD4C-TNF against L929 mouse fibroblasts was tested as described (25). To test the cytotoxicity of TNF and RGD4C-TNF against tumor cells, U87MG, MDA-MB-435, or C6 cells were plated into 96-well plates at a density of 4×10^3 cells/well and allowed to adhere overnight before adding TNF or RGD4C-TNF. After 72 h, the effects of TNF and RGD4C-TNF on the growth of tumor cells were determined using crystal violet staining (20). Plates were read on a TECAN microplate reader (Tecan Trading) at 570 nm. Each sample was analyzed in triplicate at serial dilutions. The results were expressed as mean ± SD of two independent assays. The IC_{50} values were calculated using GraphPad Prism software (GraphPad Software).

DOTA Conjugation and Radiolabeling

DOTA was activated by EDC and SNHS at pH 5.5 for 30 min with a molar ratio of 10:5:4 (DOTA/EDC/SNHS; ref. 26). The DOTA-*N*-hydroxysulfosuccinimidyl was cooled to 4°C and added to TNF or RGD4C-TNF at a molar ratio of DOTA-*N*-hydroxysulfosuccinimidyl/protein = 5:1. The reaction mixture was adjusted to pH 8.5 with 0.1 N NaOH and allowed to incubate overnight at 4°C. The DOTA-RGD4C-TNF and DOTA-TNF conjugates were purified using PD-10 column. For radiolabeling, $^{64}CuCl_2$ was diluted in 0.1 mol/L sodium acetate buffer (NaOAc, pH 6.5) and added to DOTA-TNF or DOTA-RGD4C-TNF (3.7 MBq ^{64}Cu activity/μg protein conjugate). The reaction mixture was incubated for 1 h at 40°C with constant shaking and the resulting ^{64}Cu-DOTA-TNF or ^{64}Cu-DOTA-RGD4C-TNF was purified by PD-10 column. The radioactive fractions containing ^{64}Cu-DOTA-TNF or ^{64}Cu-DOTA-RGD4C-TNF were collected and passed through a 0.2 μm low protein binding syringe filter for *in vivo* experiments. The average number of DOTA chelators per RGD4C-TNF was determined as described (26, 27).

Integrin Receptor Binding Assay

The integrin $\alpha_v\beta_3$ binding affinities of RGD4C, RGD4C-TNF, TNF, and DOTA-RGD4C-TNF were analyzed via displacement cell-binding assays using [^{125}I]echistatin as the integrin-specific radioligand (28). Experiments were done on human glioblastoma U87MG cell line. The best-fit IC_{50} values for U87MG cells were calculated by fitting the data with nonlinear regression using GraphPad Prism (GraphPad Software). Experiments were done with triplicate samples.

MicroPET Imaging Studies

Detailed microPET imaging procedure has been reported previously using a microPET R4 rodent model scanner (Siemens Medical Solutions; ref. 29). Briefly, tumor-bearing mice were anesthetized with 2% isofluorane, injected with 100 ~ 200 μCi ^{64}Cu-DOTA-RGD4C-TNF or ^{64}Cu-DOTA-TNF via tail vein, and placed in the prone position near the center of the field of view, where the highest image resolution and sensitivity are available. Five- to 10-min static scans were acquired at 1, 4, and 16 h after injection. For each microPET scan, three-dimensional regions of interest were drawn over the tumor, liver, kidneys, and muscle on decay-corrected whole-body coronal images. The average radioactivity concentration (accumulation) within a tumor or an organ was obtained from mean pixel values within the region of interest volume, which were converted to counts/mL/min by using a conversion factor. Assuming a tissue density of 1 g/mL, the counts/mL/min were converted to counts/g/min and then divided by the injected dose to obtain an imaging region of interest–derived %ID/g (30). For receptor-blocking experiments, tumor-bearing mice were imaged at 1 h after administration of 150 μCi ^{64}Cu-DOTA-RGD4C-TNF coinjected with 10 mg/kg c(RGDyK), 4 mg/kg TNF, or 10 mg/kg c(RGDyK) plus 4 mg/kg TNF.

TNFR Expression Analysis

Total RNA of tumor cell lines and tumor tissues were extracted using RNeasy Mini Kit (Qiagen) according to manufacturer's instructions. The purity and concentration of the RNA were determined by spectrophotometric methods. A total of 1 μg RNA from each cell line or tumor tissue was used in reverse transcription reaction using SuperScript III First-Strand Synthesis System for Reverse Transcription-PCR (Invitrogen). The integrity of the cDNA was examined by the expression of the glyceraldehyde-3-phosphate dehydrogenase housekeeping gene. For amplification by PCR, we used the primer pairs 5′-ACCA-AGTGCCACAAAGGAAC-3′ and 5′-CTGCAATTGAAG-CACTGGAA-3′ for hTNFR1 and 5′-TTCGCTCTTCCAG-TTGGACT-3′ and 5′-CACCAGGGGAAGAATCTGAG-3′ for hTNFR2. The PCR products were visualized on agarose gel with ethidium bromide staining.

Western blot was done using a previously described method (31). The fresh tissue extract samples (50 μg/lane) were separated by SDS-PAGE and transferred electrostatically to NC membranes. The membranes were blocked with 5% nonfat milk in TBS-T [50 mmol/L Tris (pH 7.5), 0.9% NaCl, 0.1% Tween 20] for 1 h at room temperature, and then incubated for 2 h at room temperature with a rabbit anti-human hTNFR1 antibody (1:500) or mouse anti-human hTNFR2 antibody (1:500). The membranes were washed, incubated with horseradish peroxidase–conjugated goat anti-rabbit or goat anti-mouse IgG, and then developed with an ECL advanced chemiluminescence reagent using a Kodak image station 2000R (Eastman Kodak).

In vivo Efficacy Study

Athymic nude (*nu/nu*) mice (4-6 weeks old) were injected with 5×10^6 MDA-MB-435 log-phase cells into the right mammary fat pad. When the tumors were ~50 to 100 mm^3 (2 weeks after inoculation), the mice were divided into three groups ($n = 5$) and injected i.v. through the tail vein daily for 5 days with saline, RGD4C-TNF (0.25 mg/kg), or TNF (0.25 mg/kg). The tumors were monitored every other day with a caliper for 2 weeks. Tumor volume was calculated with the formula: tumor volume = (width)^2 × length / 2 (32).

Ex vivo Staining

At the end of the therapy, mice were sacrificed and the tumors were incised and fixed with IHC Zinc Fixative (BD Bioscience). H&E staining was done as reported. For immunostaining, the tumors were snap frozen in optical cutting temperature (Sakura Finetek USA) and kept at -80°C before staining. For Ki-67 staining, frozen tumor sections were warmed to room temperature, fixed with ice-cold acetone for 10 min, and dried in the air for 30 min. The sections were blocked with 10% goat serum, incubated with rabbit anti-mouse Ki-67 antibody (Labvision), washed, incubated with Cy3-conjugated goat anti-rabbit secondary antibody (Jackson ImmunoResearch Laboratories), mounted, and then examined under the microscope (Carl Zeiss Axiovert 200M). For terminal deoxynucleotidyl transferase–mediated dUTP nick end labeling (TUNEL) and CD31 double staining, frozen tissue slices were warmed to room temperature and the fluorescent TUNEL staining was conducted following manual instruction of *In situ* Cell Death Detection kit (Roche). After TUNEL staining, the slides were subjected to CD31 (rat anti-mouse CD31 antibody was from BD Bioscience) staining using same protocol as Ki-67 staining.

Statistical Analysis

For PET imaging, the analysis of study results was focused on the test of differences of the mean tumor uptake between ^{64}Cu-DOTA-RGD4C-TNF and ^{64}Cu-DOTA-TNF at different time points. For *in vivo* efficacy evaluation, the analysis of results was focused on the differences of the mean tumor volume among treatment groups. All tests of significance were two sided, and differences were considered statistically significant when $P < 0.05$. GraphPad Prism software was used for all analyses.

Results

Characterization of RGD4C-TNF and TNF

The gene structure of RGD4C-TNF was illustrated in Fig. 1A. The expression of RGD4C-TNF in *Escherichia coli*

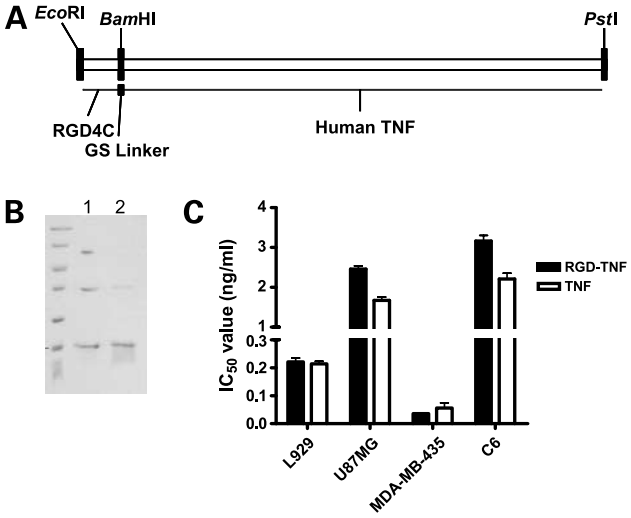

Figure 1. Production and characterization of RGD4C-TNF. **A,** gene structure of RGD4C-TNF. **B,** SDS-PAGE analysis of RGD4C-TNF. The RGD4C-TNF appeared as monomer, dimer, and trimer on nonreducing SDS-PAGE (*lane 1*) and a single monomer band under reducing condition (*lane 2*). **C,** cytolytic activity of RGD4C-TNF and TNF against L929, U87MG, MD-AMB-435, and C6 cell lines. EC_{50} values of RGD4C-TNF against U87MG, MDA-MB-435, and C6 were 2.46 ± 0.14, 0.036 ± 0.01, and 3.16 ± 0.25 ng/mL, respectively, very similar to the EC_{50} values of TNF (1.67 ± 0.15, 0.06 ± 0.03, and 2.21 ± 0.25 ng/mL against U87MG, MDA-MB-435, and C6, respectively; $P > 0.05$).

was identified by SDS-PAGE (Fig. 1B). RGD4C-TNF protein was partially soluble and the expression level of the protein was ~13%. RGD4C-TNF was purified by step-wise ammonia sulfate precipitation followed by ion-exchange chromatography. This purification procedure resulted in final yield of ~3.9 mg purified RGD4C-TNF/g cell paste. The specific activity of purified RGD4C-TNF was 2.7×10^8 units/mg. RGD4C-TNF protein could form homodimer and homotrimer under nonreducing condition. Most of the dimer and trimer were reduced to monomer and a single band at 17 kDa was shown on reduced SDS-PAGE after treatment with DTT (Fig. 1B).

Bioactivity of TNF and RGD4C-TNF

TNF bioassay on mouse L-929 cells showed that the EC_{50} value of RGD4C-TNF fusion protein (0.21 ± 0.02 ng/mL) was approximately the same as that of native TNF (Fig. 1C), suggesting that the fusion of cyclic RGD4C peptide to the NH_2 terminus of TNF did not interfere with the bioactivity of TNF. The cytolytic activity of TNF and RGD4C-TNF against various tumor cells was also examined, including $\alpha_v\beta_3$ integrin-positive U87MG human glioblastoma and MDA-MB-435 human breast cancer and $\alpha_v\beta_3$-negative C6 rat glioma cells. The EC_{50} values of RGD4C-TNF against U87MG, MDA-MB-435, and C6 were comparable with those of TNF (Fig. 1C). The level of integrin expression did not have significant effect on the bioactivity and cytotoxicity of RGD4C-TNF compared with TNF.

Binding Activity of RGD4C-TNF

The binding specificity of RGD4C-TNF was tested on integrin-positive U87MG cells using competitive displacement study. The binding of [^{125}I]echistatin to cell surface integrin $\alpha_v\beta_3$ was competed by RGD4C-TNF in a concentration-dependent manner. RGD4C-TNF fusion protein was able to fully suppress the binding of the radioligand to cell surface $\alpha_v\beta_3$ integrin. The concentration required for half-maximal competition (50% inhibitory concentration, IC_{50}) was calculated to be 247 ± 32 nmol/L, comparable with that of cyclic RGD4C peptide (379 ± 59 nmol/L). By contrast, the TNF protein is unable to inhibit the binding of [^{125}I]echistatin to $\alpha_v\beta_3$ integrin.

DOTA Conjugation and Radiolabeling

The number of DOTA per protein molecule was 0.39 ± 0.01 per RGD4C-TNF and 0.47 ± 0.01 per TNF (n = 4). U87MG cell-binding assay showed the IC_{50} value for DOTA-RGD4C-TNF was 192 ± 24 nmol/L, similar to that of RGD4C-TNF. ^{64}Cu labeling of DOTA-RGD4C-TNF and DOTA-TNF were achieved in 90 ± 10 min and the radiolabeling yield was 66.9 ± 18.1% and 59.3 ± 19.3%, respectively (n = 5). The specific activity of ^{64}Cu-DOTA-RGD4C-TNF and ^{64}Cu-DOTA-TNF was 3.7 ± 0.1 and 3.5 ± 0.1 GBq/mg, respectively (n = 5).

MicroPET Studies of ^{64}Cu-DOTA-TNF and ^{64}Cu-DOTA-RGD4C-TNF

Both ^{64}Cu-DOTA-TNF and ^{64}Cu-DOTA-RGD4C-TNF were tested in U87MG, MDA-MB-435, and C6 tumor models, and the representative decay-corrected whole-body coronal images that contain the tumors were shown in Fig. 2A. In the U87MG model that expressed high level of integrin $\alpha_v\beta_3$, tumor uptake of ^{64}Cu-DOTA-RGD4C-TNF (Fig. 2A, *a-c*, and *D, a*) was ~2-fold that of ^{64}Cu-DOTA-TNF at all time points examined (Fig. 2A, *d-f*). In the MDA-MB-435 tumor model that expressed medium level of integrin $\alpha_v\beta_3$, tumor uptake of ^{64}Cu-DOTA-RGD4C-TNF (Fig. 2A, *g-i*) was ~1.5-fold that of ^{64}Cu-DOTA-TNF (Fig. 2A, *j-k*) at all time points examined. In the integrin $\alpha_v\beta_3$-negative C6 tumor model, no significant differences between ^{64}Cu-DOTA-RGD4C-TNF (Fig. 2A, *m-o*) and ^{64}Cu-DOTA-TNF (Fig. 2A, *p-r*) were observed. The magnitude of uptake in U87MG, MDA-MB-435, and C6 tumors correlated well with the integrin expression level in these three models given that U87MG > MDA-MB-435 > C6. Both ^{64}Cu-DOTA-RGD4C-TNF and ^{64}Cu-DOTA-TNF had relatively high activity accumulation in the liver at early time points that decreased with time (30.06 ± 2.35 versus 28.19 ± 4.06, 25.51 ± 2.45 versus 24.56 ± 1.48, and 16.22 ± 1.46 versus 16.63 ± 0.55 %ID/g at 1, 4, and 20 h postinjection for ^{64}Cu-DOTA-RGD4C-TNF and ^{64}Cu-DOTA-TNF, respectively; n = 9). The expression of both TNFR1 and TNFR2 in the liver (33) and hepatic clearance were likely responsible for the persistent accumulation of ^{64}Cu-DOTA-RGD4C-TNF and ^{64}Cu-DOTA-TNF in this organ. Both ^{64}Cu-DOTA-RGD4C-TNF and ^{64}Cu-DOTA-TNF had some renal uptake that was apparently not being cleared with time (14.24 ± 0.98 versus 16.97 ± 5.50, 12.13 ± 0.85 versus 14.89 ± 4.43, and 10.73 ± 0.46 versus 12.37 ± 3.35 %ID/g at 1, 4, and 20 h postinjection for ^{64}Cu-DOTA-RGD4C-TNF and ^{64}Cu-DOTA-TNF, respectively; n = 9), presumably attributable

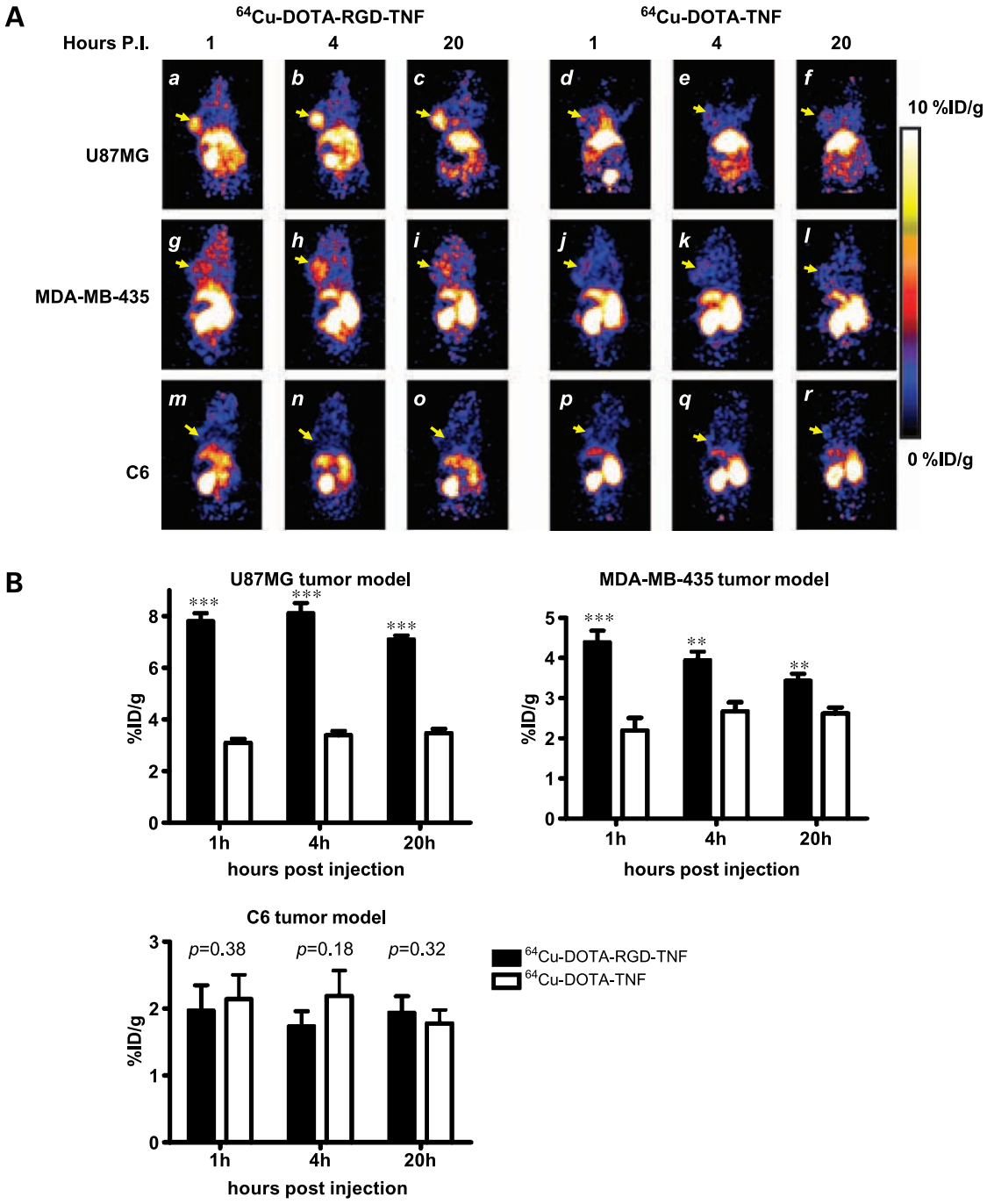

Figure 2. MicroPET study of ^{64}Cu-DOTA-RGD4C-TNF and ^{64}Cu-DOTA-TNF in tumor-bearing mice. **A,** serial microPET scans of U87MG, MDA-MB-435, and C6 tumor-bearing mice at 1, 4, and 20 h after i.v. injection of 5 to 10 MBq (~2-4 μg RGD4C-TNF) of ^{64}Cu-DOTA-RGD4C-TNF (*a-c, g-i*, and *m-o* for U87MG, MDA-MB-435, and C6, respectively). Similar amount of activity for ^{64}Cu-DOTA-TNF was also injected as a control (*d-f, j-l*, and *p-r*). For U87MG tumor model, the tumor uptake of ^{64}Cu-DOTA-RGD4C-TNF at 1, 4, and 20 h postinjection was 7.80 ± 0.67, 8.11 ± 0.88, and 7.09 ± 0.35 %ID/g, respectively, ~2-fold higher than that of ^{64}Cu-DOTA-TNF (3.10 ± 0.35, 3.39 ± 0.35, and 3.47 ± 0.39 %ID/g at 1, 4, and 20 h postinjection, respectively). In MDA-MB-435 tumor model, the tumor uptake of ^{64}Cu-DOTA-RGD4C-TNF at 1, 4, and 20 h postinjection was 4.39 ± 0.65, 3.94 ± 0.48, and 3.43 ± 0.38 %ID/g, respectively, ~1.5-fold higher than that of ^{64}Cu-DOTA-TNF (2.20 ± 0.69, 2.68 ± 0.50, and 2.62 ± 0.34 %ID/g at 1, 4, and 20 h postinjection, respectively). In contrast, in integrin-negative C6 tumor model, tumor uptake of ^{64}Cu-DOTA-RGD4C-TNF was comparable with that of ^{64}Cu-DOTA-TNF at all time point tested (e.g., 1.97 ± 0.65 versus 2.14 ± 0.63, 1.74 ± 0.39 versus 2.19 ± 0.66 and 1.94 ± 0.43 versus 1.78 ± 0.35 %ID/g at 1, 4, and 20 h postinjection for ^{64}Cu-DOTA-RGD4C-TNF and ^{64}Cu-DOTA-TNF, respectively; $n = 3$). The tumors were pointed by arrows ($n = 3$ per tracer per tumor model). **B,** bar plots illustrating the comparison of tumor uptake of ^{64}Cu-DOTA-RGD4C-TNF and ^{64}Cu-DOTA-TNF in U87MG (*a*), MDA-MB-435 (*b*), and C6 (*c*) tumor models, respectively (three mice per group). **, $P < 0.01$; ***, $P < 0.001$. For C6 group, the P values were listed in the plot. Unpaired t test was used to analyze the data. $P < 0.05$ was considered statistically significant.

to the strong expression of TNFR1 on the endothelium of glomeruli of normal kidneys(34).

Receptor Specificity of ^{64}Cu-DOTA-RGD4C-TNF

The tumor accumulation of radiolabeled RGD4C-TNF fusion protein may be due to three factors: (*a*) specific targeting mediated by interaction between RGD4C and integrin $\alpha_v\beta_3$ on tumor cells and tumor vessels, (*b*) specific targeting mediated by interaction between TNF and TNFR on the tumor cells, and (*c*) passive targeting due to enhanced permeability and retention effect as tumors have abnormal and leaky vasculature and lack of lymphatic drainage. To fully understand the *in vivo* tumor-targeting mechanism of ^{64}Cu-DOTA-RGD4C-TNF, we did serial blocking experiments in U87MG and MDA-MB-435 tumor models. As can be seen in Fig. 3, coinjection of c(RGDyK) (10 mg/kg) significantly reduced U87MG tumor uptake of ^{64}Cu-DOTA-RGD4C-TNF from 8.11 ± 0.88 to 3.51 ± 0.65 %ID/g (n = 3; P < 0.001). Coinjection of TNF protein (4 mg/kg) was also able to reduce U87MG tumor uptake to 3.63 ± 0.72 %ID/g (n = 3; P < 0.01). Coinjection of c(RGDyK) (10 mg/kg) plus TNF protein (4 mg/kg) further decreased the tumor uptake of ^{64}Cu-DOTA-RGD4C-TNF to 1.99 ± 0.13 %ID/g (n = 3; P < 0.01). Similar to that found in the U87MG tumor model, the uptake of ^{64}Cu-DOTA-RGD4C-TNF in MDA-MB-435 tumor (4.39 ± 0.65 %ID/g) was inhibited in the presence of c(RGDyK) (2.28 ± 0.07 %ID/g; n = 3; P < 0.001). TNF protein can also reduce the tumor uptake of ^{64}Cu-DOTA-RGD4C-TNF to 2.20 ± 1.07 %ID/g (n = 3; P < 0.01). The combined inhibition in the presence of RGD plus TNF was not more effective than RGD blocking alone.

The different abilities of c(RGDyK) to inhibit ^{64}Cu-DOTA-RGD4C-TNF uptake in U87MG and MDA-MB-435 tumor models prompted us to investigate the function of TNF-TNFR interaction in the accumulation of ^{64}Cu-DOTA-RGD4C-TNF in these two models. Reverse transcription-PCR

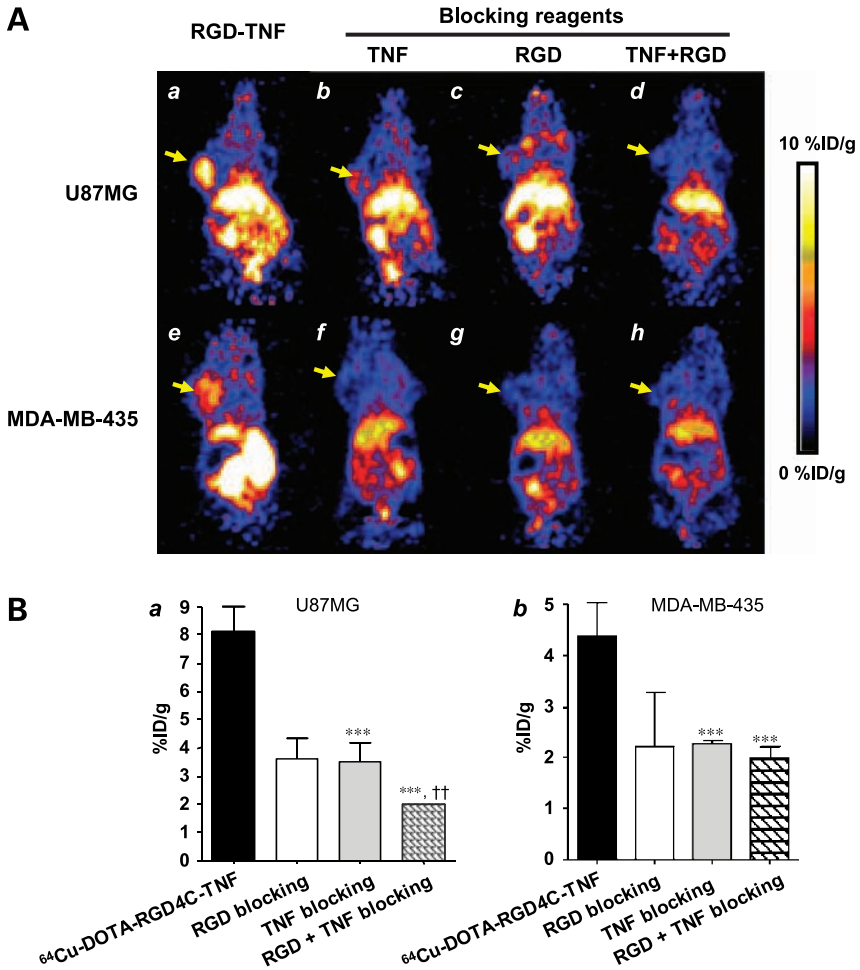

Figure 3. Receptor specificity of ^{64}Cu-DOTA-RGD4C-TNF. **A,** representative decay-corrected whole-body coronal images of female athymic nude mice bearing U87MG (*a-d*) or MDA-MB-435 (*e-h*) tumors at 1 h after i.v. injection of ^{64}Cu-DOTA-RGD4C-TNF only (*a* and *e*), with 10 mg/kg c(RGDyK) peptide (*b* and *f*), 4 mg/kg TNF protein, and 10 mg/kg c(RGDyK) plus 4 mg/kg TNF (*d* and *h*) as blocking reagents (3 mice per tumor model). **B,** quantitative microPET region of interest analysis of tumor uptake for U87MG (*a*) and MDA-MB-435 (*b*). ***, P < 0.001, compared with ^{64}Cu-DOTA-RGD4C-TNF; ††, P < 0.01, compared with RGD peptide blocking.

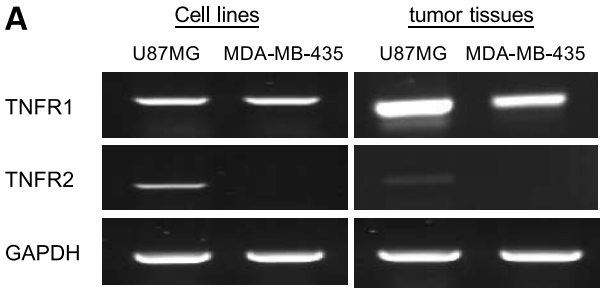

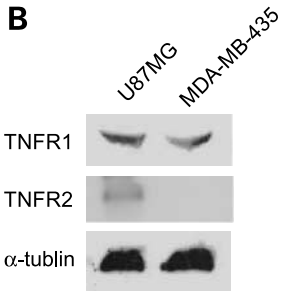

Figure 4. TNFR1 and TNFR2 expression in U87MG and MDA-MB-435 tumor cells and tumor tissues. **A,** comparison of mRNA level of TNFR in U87MG and MDA-MB-435 cell lines and tumor tissues. **B,** comparison of protein level of TNFR in U87MG and MDA-MB-435 tumor tissues.

and Western blot were done to test TNFR1 and TNFR2 expression level in both cultured U87MG and MDA-MB-435 cell lines and well-established tumor xenografts. The reverse transcription-PCR products of TNFR1, TNFR2, and glyceraldehyde-3-phosphate dehydrogenase were 263, 399, and 400 bp, respectively. As shown in Fig. 4A, TNFR1 and TNFR2 mRNA levels were higher in U87MG than in MDA-MB-435 in both cultured cells and fresh tumor tissues. This result was further confirmed by immunoblotting (Fig. 4B). The high levels of TNFR1 and TNFR2 in U87MG tumor may explain the complete blocking of ^{64}Cu-DOTA-RGD4C-TNF can only be achieved by combined c(RGDyK) and TNF in this tumor model.

In vivo Antitumor Effects of RGD4C-TNF

After the tumors were established (50-100 mm^3 in volume), MDA-MB-435 xenografted mice were divided into three groups and i.v. injected daily with saline, TNF (0.25 mg/kg), or RGD4C-TNF (0.25 mg/kg) for 5 consecutive days. The mice were observed daily for clinical symptoms and the tumor volume was measured by a digital caliper every other day. As shown in Fig. 5A, a time-related increase in tumor volume was observed in the saline-treated group in which the tumors showed an average fractional tumor volume (V/V_0) of 7.7 $\pm$ 2.4 on day 15. TNF treatment resulted in a V/V_0 of 4.3 $\pm$ 0.6 on day 15, which represents a tumor growth inhibition of 24%. RGD4C-TNF treatment resulted in a V/V_0 of 2.1 $\pm$ 1.2 on day 15, representing a tumor growth inhibition of 72%, which is significantly more effective than TNF ($P < 0.01$). Mice body weight was monitored as an indicator of toxicity of TNF. As evidenced in Fig. 5B, it is clear that neither RGD4C-TNF nor TNF has observable side effects at the low dosage used in this study.

Ex vivo Tissue Staining

In RGD4C-TNF-treated tumors, *ex vivo* tissue staining showed massive necrosis and hemorrhage (Fig. 6, *c*), decreased tumor cell proliferation (Fig. 6, *f*), and enhanced tumor cell apoptosis (Fig. 6, *l*) compared with saline (Fig. 6, *a, d*, and *j*) and TNF-treated group (Fig. 6, *b, e*, and *k*). In particular, immunofluorescent double staining of CD31 and TUNEL showed multiple overlays of CD31$^+$ and TUNEL$^+$ tumor vessels in RGD4C-TNF-treated group (Fig. 6, *o*) but not TNF-treated group (Fig. 6, *n*). These staining results showed the selective cytolytic effect of RGD4C-TNF against integrin $\alpha_v\beta_3$-positive tumor cells and tumor vessels and explained the enhanced antitumor effect of RGD4C-TNF (Supplementary Figure).[1]

Discussion

In pursuing our goal of tumor-specific delivery of cytotoxic TNF, we have constructed a fusion protein that has a cyclic RGD4C peptide moiety at the NH_2 terminus of hTNF through a glycine-serine linker. *In vitro* results showed that the RGD4C-TNF is as potent as the native TNF and has similar integrin $\alpha_v\beta_3$ binding affinity to that of RGD4C peptide. Noninvasive microPET imaging studies showed that RGD4C-TNF accumulates in tumors in an integrin $\alpha_v\beta_3$-dependent manner. The uptake of ^{64}Cu-DOTA-RGD4C-TNF is significantly higher than that of ^{64}Cu-DOTA-TNF in integrin-expressing tumors (e.g., U87MG and MDA-MB-435) but has no difference in integrin-negative tumors (e.g., C6). The uptake of ^{64}Cu-DOTA-RGD4C-TNF in integrin-positive tumors can be effectively blocked by c(RGDyK), further confirming the receptor specificity of the fusion protein *in vivo* after systemic administration. Finally, the integrin specificity of RGD4C-TNF also offers better tumoricidal capability than TNF in $\alpha_v\beta_3$-positive MDA-MB-435 breast cancer model.

It is of note that hTNF has two cysteine residues at positions 69 and 101. The intramolecular disulfide bond formed between these two cysteine plays a critical role in the biological function of TNF. The RGD4C peptide has four cysteine residues close to each other. It is a challenge to have all six cysteines to form the correct disulfide bonds for both high integrin binding affinity and potent cytolytic activity. In Fig. 1B, we did observe that, under natural conditions, a primary RGD4C-TNF monomer band and two weak dimer and trimer bands, of which the two oligomer bands disappeared under reduced condition. The formation of RGD4C-TNF oligomer is likely due to the presence of intermolecular disulfide bonds. Because RGD4C-TNF had similar cytolytic activity with TNF, it is obvious that the disulfide bond between the C69-C101 is correctly formed. In peptide ACDCRGDCDCG (RGD4C), two disulfide bonds are formed between C2-C10 and C4-C8 for optimized $\alpha_v\beta_3$ or $\alpha_v\beta_5$ binding (35). Such intermolecular

[1] Supplementary material for this article is available at Molecular Cancer Therapeutics Online (http://mct.aacrjournals.org/).

disulfide(s) are apparently maintained in the RGD motif because RGD4C-TNF showed comparable integrin binding affinity as synthetic RGD4C peptide. Because native TNF functions as a homotrimer (36, 37), the presence of trimer in the case of RGD4C-TNF may enhance the functions of this cytokine.

Many investigators have reported targeted delivery of TNF to tumor site by fusion protein strategy. However, most of these studies did not monitor the tumor-targeting efficacy and pharmacokinetics of specific molecular therapeutics. In our study, we took advantage of the ability of PET to visualize and measure the biological processes noninvasively by labeling RGD4C-TNF with positron emitting radionuclide ^{64}Cu for imaging. The medium long physical half-life of ^{64}Cu ($t_{1/2}$ = 12.7 h) is well suited for the fusion protein labeling and imaging. After identifying that RGD4C-TNF retained both binding ability to integrin $\alpha_v\beta_3$ and TNF cytolytic activity, we evaluated the tumor accumulation of ^{64}Cu-DOTA-RGD4C-TNF in three tumor models that have high (U87MG), medium (MDA-MB-435), and low (C6) integrin $\alpha_v\beta_3$ expression levels. As expected, tumor uptake of ^{64}Cu-labeled fusion protein followed the order of U87MG > MDA-MB-435 > C6. We also did several blocking experiments to elucidate the tumor-targeting mechanisms of RGD4C-TNF. First, cyclic RGD peptide c(RGDyK) was able to partially inhibit the uptake of ^{64}Cu-DOTA-RGD4C-TNF in U87MG tumors and completely inhibit the uptake of ^{64}Cu-DOTA-RGD4C-TNF in MDA-MB-435 tumors. Second, TNF protein was able to inhibit the uptake of ^{64}Cu-DOTA-RGD4C-TNF in U87MG tumor model that expresses high levels of both TNFR1 and TNFR2 as well as in MDA-MB-435 tumor model that expresses medium level of TNFR1 and very low level of TNFR2. Third, the combination of c(RGDyK) and TNF could completely block the uptake of ^{64}Cu-DOTA-RGD4C-TNF in U87MG tumor model, although such combination did not further reduce the uptake of which in MDA-MB-435 tumor model compared with studies using c(RGDyK) as single blocking agent. It appears that RGD4C moiety, despite of its apparent null effect on the cytolytic activity of TNF cytokine, does provide integrin recognition and targeting in the receptor-positive tumor *in vivo*. The expression of TNFR2 is evidently important for the *in vivo* distribution of TNF because TNFR2 has a higher affinity (K_d = 100 pmol/L) but also a faster dissociation rate ($t_{1/2}$ = 10 min) than TNFR1 (K_d = 500 pmol/L; $t_{1/2} \geq 3$ h; ref. 38). The fast off-rate of TNFR2 binding is believed to create a locally high TNF concentration at the cell surface, which in turn facilitates binding to TNFR1.

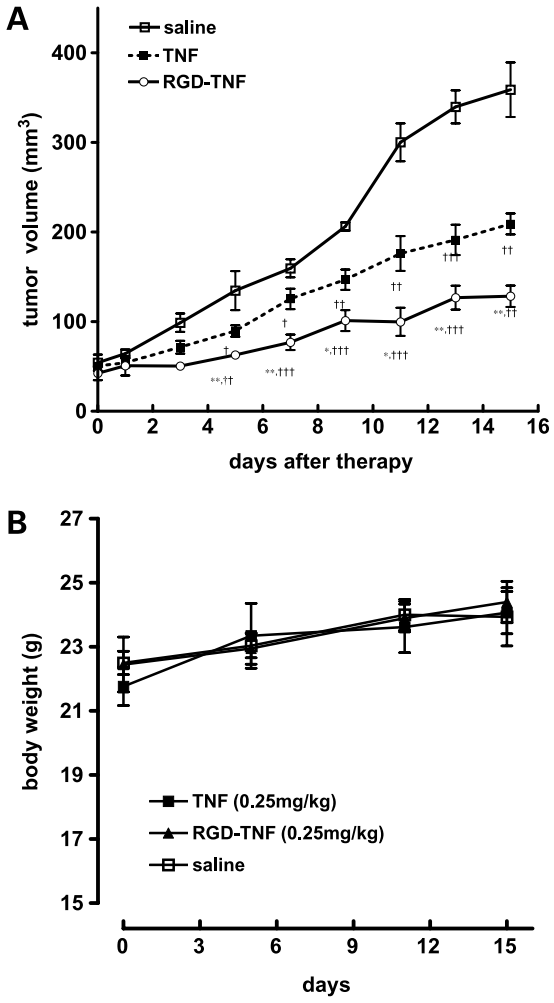

Figure 5. Antitumor effect of RGD4C-TNF in orthotopic MDA-MB-435 tumor model. **A,** 2 wk after MDA-MB-435 tumor inoculation when the tumor size reached 50 to 100 mm^3, animals (n = 5 per group) were treated i.v. for 5 consecutive days with daily injection of saline, TNF (0.25 mg/kg), or RGD4C-TNF (0.25 mg/kg). The tumor volumes were measured by a digital caliper every 2 d and compared at days 5, 7, 9, 11, 13, and 15. RGD4C-TNF versus saline (†, $P < 0.01$; †††, $P < 0.001$), RGD4C-TNF versus TNF (*, $P < 0.05$; **, $P < 0.01$; ***, $P < 0.001$), and TNF versus saline (†, $P < 0.05$; ††, $P < 0.01$; †††, $P < 0.001$). **B,** body weight of animals treated with saline, TNF, or RGD4C-TNF.

TNF is known to possess more than direct cytotoxicity against tumor cells; it also induces tumor vessel disruption (39). Our initial treatment study comparing TNF and RDG4C-TNF at a relatively low dose (0.05 mg/kg) for 5 consecutive days showed significantly better tumor-inhibitory effect of RGD4C-TNF than TNF, concurring with the pharmacokinetics studies showing that RGD4C-TNF accumulates significantly higher than TNF in the MDA-MB-435 breast cancer tumor after i.v. injection. Both TNF-treated and RGD4C-TNF-treated tumors had significant reductions in proliferative index compared with the control mice using Ki-67 analysis. TUNEL$^+$ cell analysis revealed increased DNA fragmentation and apoptosis in the treated mice compared with the control mice. Immunohistochemical analysis with 4′,6-diamidino-2-phenylindole, CD31, and TUNEL staining revealed increased apoptosis on tumor vasculature, indicating integrin-specific cytotoxicity (Supplementary Material), and tumor vasculature specific cytotoxicity of RGD4C-TNF. The combined tumor vasculature and tumor cell integrin targeting led to the impressive tumor-inhibitory effect.

We recognize several potential limitations of our study. First, our therapy study only used an integrin-expressing

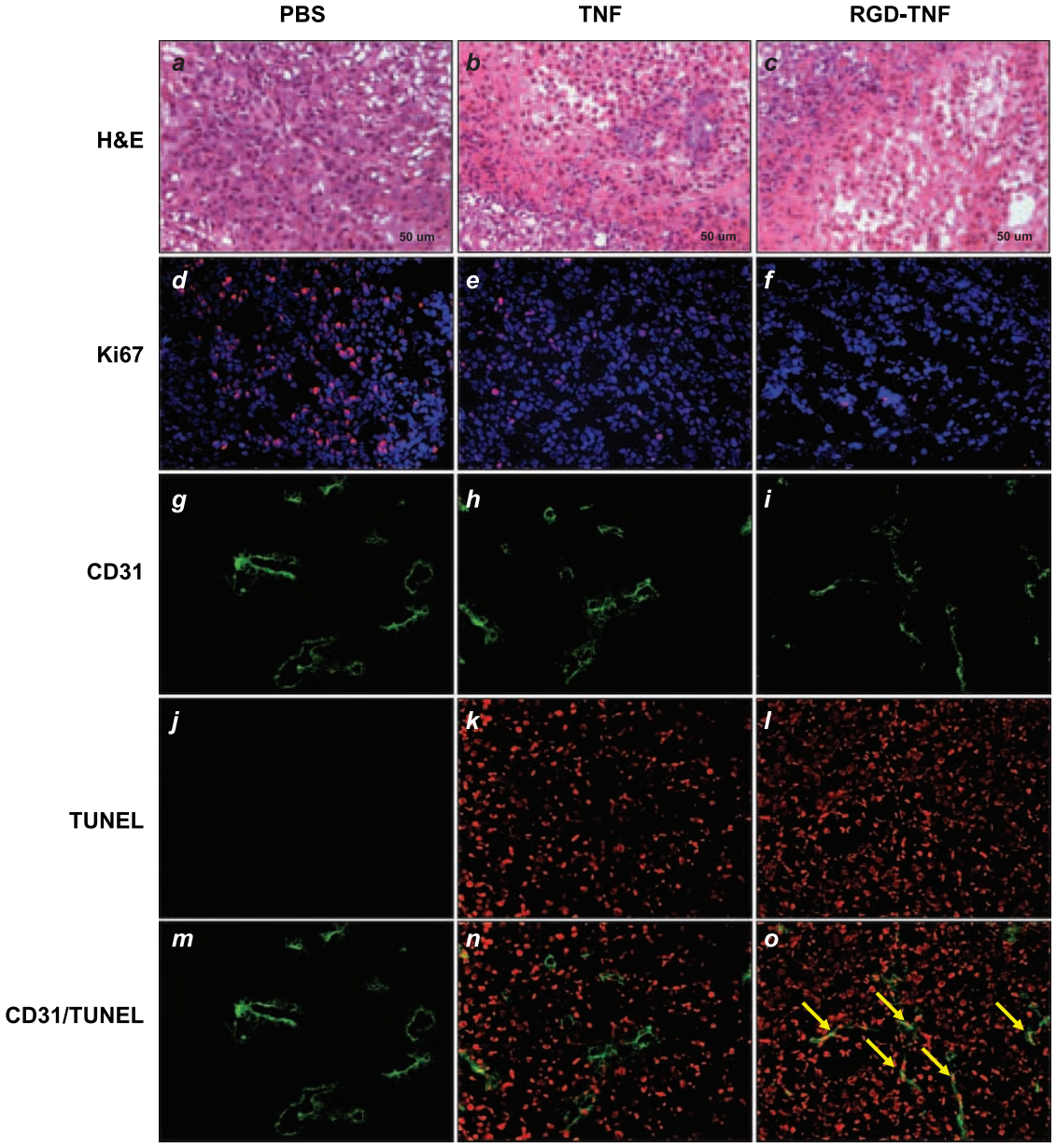

Figure 6. *Ex vivo* staining of tumor sections from saline-treated, TNF-treated, or RGD4C-TNF-treated MDA-MB-435 tumor. H&E staining (*a-c*) and immunofluorescence staining of Ki-67 (*d-f*), immunofluorescence staining of CD31 (*g-i*), TUNEL (*j-l*), and overlay (*m-o*) of the tumor sections from saline-treated, TNF-treated, and RGD-TNF-treated MDA-MB-435 tumor sections, respectively.

MDA-MB-435 tumor model. Although PET imaging, tumor size measurement, and *ex vivo* tissue staining consistently show that RGD4C-TNF induces integrin-specific tumoricidal effect, in the future, we may need to test the antitumor effect of RGD4C-TNF in an integrin $\alpha_v\beta_3$-negative tumor model, such as C6 rat glioma, to confirm that there is little or no difference between RGD4C-TNF and TNF. Second, we only selected a single dose schedule (0.05 mg/kg/d for 5 consecutive days), which is less than one-tenth of the dose used in other relevant studies. At such a low dose, TNF did not cause any normal organ toxicity (data not shown). To achieve optimal therapeutic efficacy, it will be important to determine maximum tolerated dose for native TNF and to test the difference of RGD4C-TNF and TNF in antitumor effect at high doses. Third, MDA-MB-435 tumor expresses medium levels of integrin and is highly sensitive to TNF treatment with an EC_{50} value of <0.1 ng/mL. We may want to test the same fusion protein in U87MG tumor model in future studies, as U87MG tumors are more vascular than MBA-MB-435 and express very level of integrin. In addition, U87MG cells are less sensitive to TNF and RGD4C-TNF than MDA-MB-435 cells. It will be interesting to perform

similar studies in an U87MG tumor model to assess whether integrin-targeted delivery of TNF will be better at delaying or inhibiting tumor growth.

In summary, we describe here the *in vitro* and *in vivo* characterization of RGD4C-TNF fusion protein. Incorporation of cyclic RGD4C peptide to the NH_2 terminus of TNF had little or no effect on the cytolytic toxicity effect of this cytokine. The pharmacokinetics as assessed by micro-PET imaging showed that RGD4C-TNF accumulated in the tumor through both integrin receptor and TNFR recognition. The antitumor effect of RGD4C-TNF is significantly better than TNF in integrin-positive tumor model because the fusion protein was able to selectively kill tumor vasculature and tumor cells that were integrin positive. Additional preclinical and clinical studies are warranted to optimize the therapeutic effects of this fusion protein alone and in combination with adjuvant therapies, such as 17-(allylamino)-17-demethoxygeldanamycin, to improve patient prognosis and survival.

Disclosure of Potential Conflicts of Interest

H. Wang, K. Chen, W. Cai, Z. Li, L. He, and X. Chen: Stanford University School of Medicine employees. A. Kashefi: no conflicts reported.

References

1. Locksley RM, Killeen N, Lenardo MJ. The TNF and TNF receptor superfamilies: integrating mammalian biology. Cell 2001;104:487 – 501.

2. Carswell EA, Old LJ, Kassel RL, Green S, Fiore N, Williamson B. An endotoxin-induced serum factor that causes necrosis of tumors. Proc Natl Acad Sci U S A 1975;72:3666 – 70.

3. Asher A, Mule JJ, Reichert CM, Shiloni E, Rosenberg SA. Studies on the anti-tumor efficacy of systemically administered recombinant tumor necrosis factor against several murine tumors *in vivo*. J Immunol 1987; 138:963 – 74.

4. Creasey AA, Reynolds MT, Laird W. Cures and partial regression of murine and human tumors by recombinant human tumor necrosis factor. Cancer Res 1986;46:5687 – 90.

5. Abbruzzese JL, Levin B, Ajani JA, et al. Phase I trial of recombinant human γ-interferon and recombinant human tumor necrosis factor in patients with advanced gastrointestinal cancer. Cancer Res 1989;49:4057 – 61.

6. Blick M, Sherwin SA, Rosenblum M, Gutterman J. Phase I study of recombinant tumor necrosis factor in cancer patients. Cancer Res 1987; 47:2986 – 9.

7. Grunhagen DJ, de Wilt JH, Graveland WJ, Verhoef C, van Geel AN, Eggermont AM. Outcome and prognostic factor analysis of 217 consecutive isolated limb perfusions with tumor necrosis factor-α and melphalan for limb-threatening soft tissue sarcoma. Cancer 2006;106:1776 – 84.

8. Grunhagen DJ, de Wilt JH, ten Hagen TL, Eggermont AM. Technology insight: utility of TNF-α-based isolated limb perfusion to avoid amputation of irresectable tumors of the extremities. Nat Clin Pract Oncol 2006;3:94 – 103.

9. Manusama ER, Nooijen PT, Ten Hagen TL, et al. Tumor necrosis factor-α in isolated perfusion systems in the treatment of cancer: the Rotterdam preclinical-clinical program. Semin Surg Oncol 1998;14:232 – 7.

10. Eggermont AM. TNFα in isolated perfusion systems: success in the limb, developments for the liver credits, debits and future perspectives. Anticancer Res 1998;18:3899 – 905.

11. Nakamoto T, Inagawa H, Takagi K, Soma G. A new method of antitumor therapy with a high dose of TNF perfusion for unresectable liver tumors. Anticancer Res 2000;20:4087 – 96.

12. Liu Y, Cheung LH, Marks JW, Rosenblum MG. Recombinant single-chain antibody fusion construct targeting human melanoma cells and containing tumor necrosis factor. Int J Cancer 2004;108:549 – 57.

13. Veenendaal LM, Jin H, Ran S, et al. *In vitro* and *in vivo* studies of a VEGF121/rGelonin chimeric fusion toxin targeting the neovasculature of solid tumors. Proc Natl Acad Sci U S A 2002;99:7866 – 71.

14. Halin C, Gafner V, Villani ME, et al. Synergistic therapeutic effects of a tumor targeting antibody fragment, fused to interleukin 12 and to tumor necrosis factor α. Cancer Res 2003;63:3202 – 10.

15. Liu Y, Zhang W, Cheung LH, et al. The antimelanoma immunocytokine scFvMEL/TNF shows reduced toxicity and potent antitumor activity against human tumor xenografts. Neoplasia 2006;8:384 – 93.

16. Corti A, Ponzoni M. Tumor vascular targeting with tumor necrosis factor α and chemotherapeutic drugs. Ann N Y Acad Sci 2004;1028:104 – 12.

17. Curnis F, Gasparri A, Sacchi A, Longhi R, Corti A. Coupling tumor necrosis factor-α with α_v integrin ligands improves its antineoplastic activity. Cancer Res 2004;64:565 – 71.

18. Curnis F, Sacchi A, Borgna L, Magni F, Gasparri A, Corti A. Enhancement of tumor necrosis factor α antitumor immunotherapeutic properties by targeted delivery to aminopeptidase N (CD13). Nat Biotechnol 2000;18:1185 – 90.

19. Luo YQ, Wang LH, Ma XL, Kong JX, Jiao BH. Construction, expression, and characterization of a new targeted bifunctional fusion protein: tumstatin45-132-TNF. IUBMB Life 2006;58:647 – 53.

20. Wang H, Yan Z, Shi J, Han W, Zhang Y. Expression, purification, and characterization of a neovasculature targeted rmhTNF-α in *Escherichia coli*. Protein Expr Purif 2006;45:60 – 5.

21. Felding-Habermann B, Fransvea E, O'Toole TE, Manzuk L, Faha B, Hensler M. Involvement of tumor cell integrin $\alpha_v\beta_3$ in hematogenous metastasis of human melanoma cells. Clin Exp Metastasis 2002;19:427 – 36.

22. Tucker GC. Integrins: molecular targets in cancer therapy. Curr Oncol Rep 2006;8:96 – 103.

23. Cao Q, Cai W, Li T, et al. Combination of integrin siRNA and irradiation for breast cancer therapy. Biochem Biophys Res Commun 2006;351:726 – 32.

24. Cai W, Chen X. Anti-angiogenic cancer therapy based on integrin $\alpha_v\beta_3$ antagonism. Anticancer Agents Med Chem 2006;6:407 – 28.

25. Corti A, Poiesi C, Merli S, Cassani G. Tumor necrosis factor (TNF) α quantification by ELISA and bioassay: effects of TNFα-soluble TNF receptor (p55) complex dissociation during assay incubations. J Immunol Methods 1994;177:191 – 8.

26. Cai W, Wu Y, Chen K, Cao Q, Tice DA, Chen X. *In vitro* and *in vivo* characterization of 64Cu-labeled Abegrin, a humanized monoclonal antibody against integrin $\alpha_v\beta_3$. Cancer Res 2006;66:9673 – 81.

27. Meares CF, McCall MJ, Reardan DT, Goodwin DA, Diamanti CI, McTigue M. Conjugation of antibodies with bifunctional chelating agents: isothiocyanate and bromoacetamide reagents, methods of analysis, and subsequent addition of metal ions. Anal Biochem 1984;142:68 – 78.

28. Wu Y, Zhang X, Xiong Z, et al. microPET imaging of glioma integrin $\alpha_v\beta_3$ expression using ^{64}Cu-labeled tetrameric RGD peptide. J Nucl Med 2005;46:1707 – 18.

29. Zhang X, Xiong Z, Wu Y, et al. Quantitative PET imaging of tumor integrin $\alpha_v\beta_3$ expression with ^{18}F-FRGD2. J Nucl Med 2006;47:113 – 21.

30. Cao Q, Cai W, Li ZB, et al. PET imaging of acute and chronic inflammation in living mice. Eur J Nucl Med Mol Imaging 2007;34:1832 – 42.

31. Cai W, Chen K, Mohamedali KA, et al. PET of vascular endothelial growth factor receptor expression. J Nucl Med 2006;47:2048 – 56.

32. Osborne CK, Hobbs K, Clark GM. Effect of estrogens and antiestrogens on growth of human breast cancer cells in athymic nude mice. Cancer Res 1985;45:584 – 90.

33. Schumann J, Bluethmann H, Tiegs G. Synergism of *Pseudomonas aeruginosa* exotoxin A with endotoxin, superantigen, or TNF results in TNFR1- and TNFR2-dependent liver toxicity in mice. Immunol Lett 2000; 74:165 – 72.

34. Al-Lamki RS, Wang J, Skepper JN, Thiru S, Pober JS, Bradley JR. Expression of tumor necrosis factor receptors in normal kidney and rejecting renal transplants. Lab Invest 2001;81:1503 – 15.

35. Koivunen E, Wang B, Ruoslahti E. Phage libraries displaying cyclic peptides with different ring sizes: ligand specificities of the RGD-directed integrins. Biotechnology NY 1995;13:265 – 70.

36. Narachi MA, Davis JM, Hsu YR, Arakawa T. Role of single disulfide in recombinant human tumor necrosis factor-α. J Biol Chem 1987;262:3107 – 10.

37. Menart V, Gaberc-Porekar V, Jevsevar S, Pernus M, Meager A, Stalc A. Early events in TNFa-p55 receptor interactions—experiments with TNF dimers. Pflugers Arch 2000;439:R113 – 5.

38. Herbein G, O'Brien WA. Tumor necrosis factor (TNF)-α and TNF receptors in viral pathogenesis. Proc Soc Exp Biol Med 2000;223:241 – 57.

39. Watanabe N, Niitsu Y, Umeno H, et al. Toxic effect of tumor necrosis factor on tumor vasculature in mice. Cancer Res 1988;48:2179 – 83.